Evaluating higher moments in the transverse Kelvin–Helmholtz instability by full kinetic simulation

Takayuki Umeda (iD)

View Online   Export Citation   CrossMark

ARTICLES YOU MAY BE INTERESTED IN

Evaluating higher moments in the transverse Kelvin–Helmholtz instability by full kinetic simulation

View Online Export Citation CrossMark

Takayuki Umeda[a] iD

AFFILIATIONS

Institute for Space-Earth Environmental Research, Nagoya University, Nagoya 464-8601, Japan

[a]Author to whom correspondence should be addressed: taka.umeda@nagoya-u.jp

ABSTRACT

Approximated forms of the third and fourth moments of a velocity distribution function are derived by using a perturbed velocity distribution function around a characteristic spatial scale on the gyroradius derived by Thompson [Rep. Prog. Phys. **24**, 363–424 (1961)]. Then, they are evaluated by using a two-dimensional full kinetic Vlasov simulation result of the transverse Kelvin–Helmholtz instability. It is shown that the derived form of the fourth moment is in agreement with the one calculated from the distribution function data of the Vlasov simulation. On the other hand, the derived form of the third moment is quite different from the one (i.e., heat flux tensor) calculated from the distribution function data of the Vlasov simulation. The results suggest that the perturbed velocity distribution function of Thompson needs an improvement.

Published under license by AIP Publishing. https://doi.org/10.1063/1.5139442

I. INTRODUCTION

Non-magneto-hydro-dynamic (MHD) effects on various plasma processes are fundamental issues in plasma physics. Recent studies of magneto-hydro-dynamic (MHD) instabilities at boundary layers by using fully kinetic simulations indicated the importance of higher moments for reproducing (approximating) full kinetic simulation results by fluid simulations.[1–3] In the MHD equation, the following scalar energy (or pressure) equation is conventionally solved, in which the scalar pressure P is defined as the trace of the pressure tensor $\mathbf{P}$:

$$\frac{\partial}{\partial t}\left(m_i N|\mathbf{U}|^2 + \frac{2}{\gamma-1}P\right)$$
$$= -\nabla \cdot (m_i N|\mathbf{U}|^2 \mathbf{U}) - \frac{2\gamma}{\gamma-1}\nabla \cdot (P\mathbf{U}) + 2\mathbf{E} \cdot \mathbf{J}. \quad (1)$$

Here, the off-diagonal pressure (i.e., stress) terms are neglected in the energy/pressure equation. The heat capacity ratio γ is given by $\gamma = (D+2)/D$, where D is the number of velocity dimensions. Note that the density N, the fluid bulk velocity vector $\mathbf{U}$, and the pressure tensor $\mathbf{P}$ are given by taking the zeroth, first, and second moments of a velocity distribution function f as follows:

$$N = \iiint f \,\mathrm{d}^3\mathbf{v}, \quad (2)$$

$$\mathbf{U} = \frac{1}{N}\iiint \mathbf{v} f \,\mathrm{d}^3\mathbf{v}, \quad (3)$$

$$\mathbf{P} = m\iiint (\mathbf{v}-\mathbf{U})(\mathbf{v}-\mathbf{U}) f \,\mathrm{d}^3\mathbf{v}, \quad (4)$$

where $\mathbf{vv}$ represents a dyadic product.

The pressure equation, including the pressure tensor $\mathbf{P}$ and the heat flux vector $\mathbf{Q}$, is written as follows:

$$\frac{\partial P}{\partial t} = -\nabla \cdot (P\mathbf{U}) - (\gamma-1)(\mathbf{P}\nabla) \cdot \mathbf{U} - \frac{\gamma-1}{2}\nabla \cdot \mathbf{Q}$$
$$= -\nabla \cdot (P\mathbf{U}) - (\gamma-1)P\nabla \cdot \mathbf{U}$$
$$- (\gamma-1)(\mathbf{\Pi}\nabla) \cdot \mathbf{U} - \frac{\gamma-1}{2}\nabla \cdot \mathbf{Q}, \quad (5)$$

where $\mathbf{P} = P\mathbf{I} + \mathbf{\Pi}$, with $\mathbf{I}$ and $\mathbf{\Pi}$ being the unit tensor and the stress tensor, respectively. The heat flux vector is defined as

$$\mathbf{Q} = m\iiint |\mathbf{v}-\mathbf{U}|^2(\mathbf{v}-\mathbf{U}) f \,\mathrm{d}^3\mathbf{v}. \quad (6)$$

Note that $\mathbf{P}\nabla$ and $\mathbf{\Pi}\nabla$ are matrix products.

Let us consider a four-dimensional phase space with two spatial and two velocity dimensions (x, y, v_x, v_y), in which the ambient magnetic field is taken only in the z direction (B_z). Then, the out-of-plane

current density J_z component does not play any role on the MHD scale in the present coordinate system, because the current density J_z component (which is exactly parallel to the ambient magnetic field) is responsive to the ordinary light-mode waves only.

According to Thompson,[4] the pressure tensor for the species s in the present coordinate system ($\gamma = 2$) is approximated as follows:

$$P_{xxs} \approx P_s - \frac{P_s}{2\omega_{cs}}\left(\frac{\partial U_{ys}}{\partial x} + \frac{\partial U_{xs}}{\partial y}\right), \qquad (7)$$

$$P_{yys} \approx P_s + \frac{P_s}{2\omega_{cs}}\left(\frac{\partial U_{ys}}{\partial x} + \frac{\partial U_{xs}}{\partial y}\right), \qquad (8)$$

$$P_{xys} = P_{yxs} \approx \frac{P_s}{2\omega_{cs}}\left(\frac{\partial U_{xs}}{\partial x} - \frac{\partial U_{ys}}{\partial y}\right), \qquad (9)$$

where $P \equiv (P_{xx} + P_{yy})/2$ represents the scalar pressure and $\omega_{cs} \equiv q_s B_z/m_s$ represents the gyrofrequency with a sign included to consider the direction of the ambient magnetic field B_z. Then, the stress tensor Π is approximated as follows:

$$\Pi_{xxs} = -\Pi_{yys} = -\frac{P_s}{2\omega_{cs}}\left(\frac{\partial U_{ys}}{\partial x} + \frac{\partial U_{xs}}{\partial y}\right), \qquad (10)$$

$$\Pi_{xys} = \Pi_{yxs} = \frac{P_s}{2\omega_{cs}}\left(\frac{\partial U_{xs}}{\partial x} - \frac{\partial U_{ys}}{\partial y}\right). \qquad (11)$$

It is easy to find that $(P_{xx} - P_{yy})/2 = \Pi_{xx} = -\Pi_{yy}$. The approximated stress tensor is known as the stress viscosity and is later known as the Finite Larmor Radius (FLR) term[5] or the gyroviscosity as well. A recent analysis has (re)confirmed that the stress viscosity in Eqs. (10) and (11) was a good approximation of the stress tensor in the Kelvin–Helmholtz instability (KHI).[1]

The KHI is focused on in the present study because of its impact on observational, theoretical, and numerical plasma physics. The KHI, which grows in a velocity shear layer, is one of fundamental processes for the exchange of mass, momentum, and energy in collisionless plasma.[6–11] *In situ* spacecraft observations have shown an evidence of rolled-up vortices around the Earth's low-latitude magnetospheric boundary where there exists the velocity shear between the solar wind flowing plasma and the magnetospheric plasma at rest, which indicates the development of the KHI.[12–17] Secondary velocity/density shear layers formed in KH vortices are able to become a free energy source for various secondary instabilities, such as Rayleigh-Taylor instability,[18–20] magneto-rotational instability,[21] current sheet kink instability,[22] and lower-hybrid drift instability.[23] Magnetic reconnection or tearing instability is also generated when the in-plane components of the ambient magnetic field [i.e., (B_x, B_y)] exist initially,[24–30] which is, however, out of scope of the present study because the present two-dimensional coordinate system without in-plane magnetic fields is not able to treat the development of the out-of-plane component of current density (J_z) and electric field (E_z).

Recent fully kinetic simulations of fluid instabilities at MHD-scale boundary layers showed that there is asymmetry in the development of the scalar pressure depending on the orientation of the inner product between the vorticity of the primary velocity shear layer, $\mathbf{\Omega} = \nabla \times \mathbf{U}$, and the magnetic field vector $\mathbf{B}$ (e.g., Refs. 1 and 2). This phenomenon in the KHI has been studied in terms of the dawn–dusk asymmetry at Earth's magnetosphere, where $\mathbf{\Omega} \cdot \mathbf{B}$ is positive at the dusk-side low-latitude magnetospheric boundary but is negative at the dawn-side low-latitude magnetospheric boundary.[31–39]

If the stress tensor is well approximated by the gyroviscosity in Eqs. (10) and (11), then the term $(\Pi\nabla) \cdot \mathbf{U}$ in Eq. (5) is zero. It is indicated that the asymmetric development of the scalar pressure depending on the polarity of $\mathbf{\Omega} \cdot \mathbf{B}$ is due to the heat flux term $\nabla \cdot \mathbf{Q}$. Hence, the purpose of this study is twofold. One is to derive the approximated form of the third moment (i.e., heat flux tensor) $\mathbf{Q}$ and the fourth moment $\mathbf{R}$ based on the procedure of Thompson.[4] The other is to evaluate the derived approximated form of the third and fourth moments by using two-dimensional full kinetic simulation data of the transverse KHI. It should be noted that it has now become possible to make direct comparison between past theories and full Vlasov simulations owing to the development of both supercomputer technologies and multi-dimensional Vlasov simulation techniques.

II. THEORETICAL FORMULATION

We start from Eq. (4.50) in Ref. 4, which is given in the following equation in the present coordinate system:

$$f_1 \approx \frac{1}{\omega_c}\left\{ \underbrace{c_y\left(\frac{\partial f}{\partial x} - 2\frac{\partial f}{\partial c_\perp^2}\frac{dU_x}{dt}\right) - c_x\left(\frac{\partial f}{\partial y} - 2\frac{\partial f}{\partial c_\perp^2}\frac{dU_y}{dt}\right)}_{(a)} \right.$$
$$\left. \times \underbrace{- c_x c_y \frac{\partial f}{\partial c_\perp^2}\left(\frac{\partial U_x}{\partial x} - \frac{\partial U_y}{\partial y}\right) - \frac{c_y^2 - c_x^2}{2}\frac{\partial f}{\partial c_\perp^2}\left(\frac{\partial U_x}{\partial y} + \frac{\partial U_y}{\partial x}\right)}_{(b)} \right\}.$$
$$(12)$$

Here, the velocity coordinate perpendicular to the magnetic field, (c_x, c_y), is defined as the cylindrical coordinate centered at the fluid bulk velocity (U_x, U_y), i.e., $(c_x, c_y) \equiv (v_x - U_x, v_y - U_y) = c_\perp(\cos\theta, \sin\theta)$. Equation (12) was derived by Thompson[4] from the Taylor expansion of the Vlasov equation around a characteristic spatial scale on the gyroradius, in which the velocity distribution function f was separated into a gyrotropic part f_0 (i.e., $\partial f_0/\partial\theta = 0$) and a non-gyrotropic and perturbed part (in the θ direction) f_1,[4] i.e., $f \approx f_0 + f_1$. One can easily find that Eqs. (7), (8), and (9) are obtained by $\int\int c_x^2 f d^2\mathbf{v}$, $\int\int c_y^2 f d^2\mathbf{v}$, and $\int\int c_x c_y f d^2\mathbf{v}$, respectively, by using Eq. (12).

The third moment (i.e., heat flux tensor) $\mathbf{Q}$ and the fourth moment $\mathbf{R}$ are defined (e.g., Refs. 40 and 41) as follows:

$$\mathbf{Q} = m\int\int\int(\mathbf{v} - \mathbf{U})(\mathbf{v} - \mathbf{U})(\mathbf{v} - \mathbf{U})f d^3\mathbf{v}, \qquad (13)$$

$$\mathbf{R} = m\int\int\int(\mathbf{v} - \mathbf{U})(\mathbf{v} - \mathbf{U})(\mathbf{v} - \mathbf{U})(\mathbf{v} - \mathbf{U})f d^3\mathbf{v}. \qquad (14)$$

By using Eq. (12), the approximated form of the heat flux tensor $\mathbf{Q}$ is calculated by taking the third moment of the velocity distribution function as follows:

$$Q_{xxx} \equiv m\int\int c_x^3 f d^2\mathbf{v}$$
$$\approx -\frac{m}{\omega_c}\int\int\left(c_\perp^4\cos^4\theta\frac{\partial f}{\partial y} - c_\perp^3\cos^4\theta\frac{\partial f}{\partial c_\perp}\frac{dU_y}{dt}\right)c_\perp dc_\perp d\theta$$
$$= -\frac{3\pi m}{4\omega_c}\int\left(c_\perp^5\frac{\partial f}{\partial y} + 4c_\perp^3 f\frac{dU_y}{dt}\right)dc_\perp = -\frac{3}{2\omega_c}\frac{\partial R}{\partial y} - \frac{3P}{\omega_c}\frac{dU_y}{dt},$$
$$(15)$$

$$Q_{xxy} \equiv m \iint c_x^2 c_y f \mathrm{d}^2\boldsymbol{v}$$

$$\approx \frac{m}{\omega_c} \iint \left(c_\perp^4 \cos^2\theta \sin^2\theta \frac{\partial f}{\partial x} - c_\perp^3 \cos^2\theta \sin^2\theta \frac{\partial f}{\partial c_\perp}\frac{\mathrm{d}U_x}{\mathrm{d}t} \right) c_\perp \mathrm{d}c_\perp \mathrm{d}\theta$$

$$= \frac{\pi m}{4\omega_c} \int \left(c_\perp^5 \frac{\partial f}{\partial x} + 4c_\perp^3 f \frac{\mathrm{d}U_x}{\mathrm{d}t} \right) \mathrm{d}c_\perp = \frac{1}{2\omega_c}\frac{\partial R}{\partial x} + \frac{P}{\omega_c}\frac{\mathrm{d}U_x}{\mathrm{d}t} = \frac{Q_{yyy}}{3}, \tag{16}$$

$$Q_{xyy} \equiv m \iint c_x c_y^2 f \mathrm{d}^2\boldsymbol{v}$$

$$\approx -\frac{m}{\omega_c} \iint \left(c_\perp^4 \cos^2\theta \sin^2\theta \frac{\partial f}{\partial y} - c_\perp^3 \cos^2\theta \sin^2\theta \frac{\partial f}{\partial c_\perp}\frac{\mathrm{d}U_y}{\mathrm{d}t} \right) c_\perp \mathrm{d}c_\perp \mathrm{d}\theta$$

$$= -\frac{\pi m}{4\omega_c} \int \left(c_\perp^5 \frac{\partial f}{\partial y} + 4c_\perp^3 f \frac{\mathrm{d}U_y}{\mathrm{d}t} \right) \mathrm{d}c_\perp$$

$$= -\frac{1}{2\omega_c}\frac{\partial R}{\partial y} - \frac{P}{\omega_c}\frac{\mathrm{d}U_y}{\mathrm{d}t} = \frac{Q_{xxx}}{3}, \tag{17}$$

$$Q_{yyy} \equiv m \iint c_y^3 f \mathrm{d}^2\boldsymbol{v}$$

$$\approx \frac{m}{\omega_c} \iint \left(c_\perp^4 \sin^4\theta \frac{\partial f}{\partial x} - c_\perp^3 \sin^4\theta \frac{\partial f}{\partial c_\perp}\frac{\mathrm{d}U_x}{\mathrm{d}t} \right) c_\perp \mathrm{d}c_\perp \mathrm{d}\theta$$

$$= \frac{3\pi m}{4\omega_c} \int \left(c_\perp^5 \frac{\partial f}{\partial x} + 4c_\perp^3 f \frac{\mathrm{d}U_x}{\mathrm{d}t} \right) \mathrm{d}c_\perp = \frac{3}{2\omega_c}\frac{\partial R}{\partial x} + \frac{3P}{\omega_c}\frac{\mathrm{d}U_x}{\mathrm{d}t}, \tag{18}$$

where

$$\mathrm{d}^2\boldsymbol{v} = c_\perp \mathrm{d}c_\perp \mathrm{d}\theta,$$

$$\int c_\perp^{n+1} \frac{\partial f}{\partial c_\perp^2} \mathrm{d}c_\perp = \frac{1}{2}\int c_\perp^n \frac{\partial f}{\partial c_\perp} \mathrm{d}c_\perp = -\frac{n}{2}\int c_\perp^{n-1} f \mathrm{d}c_\perp,$$

$$P \equiv \frac{m}{2}\int 2\pi c_\perp^3 f \mathrm{d}c_\perp,$$

and

$$R \equiv \frac{m}{4}\int 2\pi c_\perp^5 f \mathrm{d}c_\perp = \frac{m}{4}\int 2\pi c_\perp (c_x^2 + c_y^2)^2 f \mathrm{d}c_\perp. \tag{19}$$

Here, the subscript s is omitted for simplicity. It is shown that the approximated form of the heat flux tensor requires the scalar values of the pressure P and the fourth moment R. It is also noted that the heat flux vector in Eq. (5) is given as $\boldsymbol{Q} \equiv (Q_{xxx} + Q_{xyy}, Q_{xxy} + Q_{yyy})$.

It is known that the fluid equation of motion is described as follows:

$$\frac{\mathrm{d}U_x}{\mathrm{d}t} = \frac{q}{m}(E_x + U_y B_z) - \frac{1}{mN}\left(\frac{\partial P_{xx}}{\partial x} + \frac{\partial P_{xy}}{\partial y}\right), \tag{20}$$

$$\frac{\mathrm{d}U_y}{\mathrm{d}t} = \frac{q}{m}(E_y - U_x B_z) - \frac{1}{mN}\left(\frac{\partial P_{xy}}{\partial x} + \frac{\partial P_{yy}}{\partial y}\right). \tag{21}$$

The approximated form of the first moment of a velocity distribution function by using Eq. (12) was derived by Thompson[4] as

$$\iint c_x f \mathrm{d}^2\boldsymbol{v} \approx -\frac{1}{\omega_c}\iint \left(c_\perp^3 \frac{\partial f}{\partial y} - c_\perp^2 \frac{\partial f}{\partial c_\perp}\frac{\mathrm{d}U_y}{\mathrm{d}t} \right) \cos^2\theta \mathrm{d}c_\perp \mathrm{d}\theta$$

$$= -\frac{1}{2m\omega_c}\left(\frac{\partial P}{\partial y} + mN\frac{\mathrm{d}U_y}{\mathrm{d}t}\right), \tag{22}$$

$$\iint c_y f \mathrm{d}^2\boldsymbol{v} \approx \frac{1}{\omega_c}\iint \left(c_\perp^3 \frac{\partial f}{\partial x} - c_\perp^2 \frac{\partial f}{\partial c_\perp}\frac{\mathrm{d}U_x}{\mathrm{d}t} \right) \sin^2\theta \mathrm{d}c_\perp \mathrm{d}\theta$$

$$= \frac{1}{2m\omega_c}\left(\frac{\partial P}{\partial x} + mN\frac{\mathrm{d}U_x}{\mathrm{d}t}\right). \tag{23}$$

However, it is obvious that the above approximated form does not become zero with the fluid equation of motion (20) and (21). Hence, we use $mN\mathrm{d}U_x/\mathrm{d}t \approx -\partial P/\partial x$ and $mN\mathrm{d}U_y/\mathrm{d}t \approx -\partial P/\partial y$, instead of Eqs. (20) and (21), for the approximation of the third moment.

By using the same procedure, we also calculate the approximated form of the fourth moment tensor $\mathbf{R}$ as

$$R_{xxxx} \equiv m \iint c_x^4 f \mathrm{d}^2\boldsymbol{v}$$

$$\approx m \iint \left\{ c_\perp^4 f \cos^4\theta - \frac{c_\perp^5}{4\omega_c}(\cos^4\theta \sin^2\theta - \cos^6\theta) \right.$$

$$\left. \times \frac{\partial f}{\partial c_\perp}\left(\frac{\partial U_x}{\partial y} + \frac{\partial U_y}{\partial x}\right) \right\} c_\perp \mathrm{d}c_\perp \mathrm{d}\theta$$

$$= 2\pi m \left\{ \frac{3}{8} + \frac{6}{4}\left(\frac{1}{16} - \frac{5}{16}\right)\frac{1}{\omega_c}\left(\frac{\partial U_x}{\partial y} + \frac{\partial U_y}{\partial x}\right) \right\}$$

$$\times \int c_\perp^5 f \mathrm{d}c_\perp = \frac{3R}{2} - \frac{3R}{2\omega_c}\left(\frac{\partial U_x}{\partial y} + \frac{\partial U_y}{\partial x}\right), \tag{24}$$

$$R_{xxxy} \equiv m \iint c_x^3 c_y f \mathrm{d}^2\boldsymbol{v}$$

$$\approx -m\frac{1}{2\omega_c}\iint \left\{ c_\perp^5 \cos^4\theta \sin^2\theta \frac{\partial f}{\partial c_\perp}\left(\frac{\partial U_x}{\partial x} - \frac{\partial U_y}{\partial y}\right) \right\} c_\perp \mathrm{d}c_\perp \mathrm{d}\theta$$

$$= \frac{3\pi m}{8\omega_c}\left(\frac{\partial U_x}{\partial x} - \frac{\partial U_y}{\partial y}\right)\int c_\perp^5 f \mathrm{d}c_\perp = \frac{3R}{4\omega_c}\left(\frac{\partial U_x}{\partial x} - \frac{\partial U_y}{\partial y}\right), \tag{25}$$

$$R_{xxyy} \equiv m \iint c_x^2 c_y^2 f \mathrm{d}^2\boldsymbol{v}$$

$$\approx m \iint \left\{ f c_\perp^4 \cos^2\theta \sin^2\theta - \frac{c_\perp^5}{4\omega_c}(\cos^4\theta \sin^2\theta - \cos^2\theta \sin^4\theta) \right.$$

$$\left. \times \frac{\partial f}{\partial c_\perp}\left(\frac{\partial U_x}{\partial y} + \frac{\partial U_y}{\partial x}\right) \right\} c_\perp \mathrm{d}c_\perp \mathrm{d}\theta$$

$$= \frac{\pi m}{4}\int c_\perp^5 f \mathrm{d}c_\perp = \frac{R}{2}, \tag{26}$$

$$R_{xyyy} \equiv m \iint c_x c_y^3 f \mathrm{d}^2\boldsymbol{v}$$

$$\approx -m\frac{1}{2\omega_c}\iint \left\{ c_\perp^5 \cos^2\theta \sin^4\theta \frac{\partial f}{\partial c_\perp}\left(\frac{\partial U_x}{\partial x} - \frac{\partial U_y}{\partial y}\right) \right\} c_\perp \mathrm{d}c_\perp \mathrm{d}\theta$$

$$= \frac{3\pi m}{8\omega_c}\left(\frac{\partial U_x}{\partial x} - \frac{\partial U_y}{\partial y}\right)\int c_\perp^5 f \mathrm{d}c_\perp = \frac{3R}{4\omega_c}\left(\frac{\partial U_x}{\partial x} - \frac{\partial U_y}{\partial y}\right), \tag{27}$$

$$R_{yyyy} \equiv m \int\int c_y^4 f \, d^2 \boldsymbol{v}$$

$$\approx m \int\int \left\{ f c_\perp^4 \sin^4\theta - \frac{c_\perp^5}{4\omega_c} \left(\sin^6\theta - \cos^2\theta \sin^4\theta \right) \right.$$

$$\left. \times \frac{\partial f}{\partial c_\perp} \left(\frac{\partial U_x}{\partial y} + \frac{\partial U_y}{\partial x} \right) \right\} c_\perp \, dc_\perp \, d\theta$$

$$= 2\pi m \left\{ \frac{3}{8} + \frac{6}{4} \left(\frac{5}{16} - \frac{1}{16} \right) \frac{1}{\omega_c} \left(\frac{\partial U_x}{\partial y} + \frac{\partial U_y}{\partial x} \right) \right\} \int c_\perp^5 f \, dc_\perp$$

$$= \frac{3R}{2} + \frac{3R}{2\omega_c} \left(\frac{\partial U_x}{\partial y} + \frac{\partial U_y}{\partial x} \right). \tag{28}$$

The scalar value of the fourth moment in Eq. (19) is also rewritten as

$$R = \frac{R_{xxxx} + 2R_{xxyy} + R_{yyyy}}{4}. \tag{29}$$

In the previous studies,[4,5] the stress tensor $\boldsymbol{\Pi} = \boldsymbol{P} - P\boldsymbol{I}$, which is the deviation from the scalar pressure, is defined for describing the second moment. For the direct comparison between these approximated forms and the moments of the velocity distribution function calculated by using the full Vlasov simulation data, we denote the approximated forms of the third and fourth moments as $\boldsymbol{\Theta}$ and $\boldsymbol{\Psi}$, respectively,

$$\Theta_{xxx} = 3\Theta_{xyy} = -\frac{3}{2\omega_c} \frac{\partial R}{\partial y} + \frac{3P}{m\omega_c N} \frac{\partial P}{\partial y}, \tag{30}$$

$$\Theta_{yyy} = 3\Theta_{xxy} = \frac{3}{2\omega_c} \frac{\partial R}{\partial x} - \frac{3P}{m\omega_c N} \frac{\partial P}{\partial x}, \tag{31}$$

$$\Psi_{xxxx} = -\Psi_{yyyy} = -\frac{3R}{2\omega_c} \left(\frac{\partial U_x}{\partial y} + \frac{\partial U_y}{\partial x} \right) \approx \frac{R_{xxxx} - R_{yyyy}}{2}, \tag{32}$$

$$\Psi_{xxxy} = \Psi_{xyyy} = \frac{3R}{4\omega_c} \left(\frac{\partial U_x}{\partial x} - \frac{\partial U_y}{\partial y} \right). \tag{33}$$

III. VLASOV SIMULATION

The purpose of the present study is to evaluate the approximated forms of the third and fourth moments by using full kinetic simulation data. In the present study, we re-performed Vlasov simulation runs with almost the same setup as the previous two-dimensional full electromagnetic Vlasov simulation study[36] to calculate the third and fourth moments of the velocity distribution function. See Ref. 36 for the detailed simulation setup and results. Here, we briefly describe the simulation setup.

The code has two spatial and two velocity dimensions[42] and is based on a non-oscillatory and conservative semi-Lagrangian scheme[43,44] with several improvements.[45–47] Detailed descriptions of the simulation code are given in the references.

The transverse KHI is driven by primary velocity and density shears given by hyperbolic tangent,

$$U_{yi}(y) = \frac{\Delta U}{2} \left\{ 1 - \tanh\left(\frac{y}{L}\right) \right\} \tag{34}$$

and

$$N_i(y) = \frac{N_{low} - N_{high}}{2} \tanh\left(\frac{y}{L}\right) + \frac{N_{low} + N_{high}}{2}, \tag{35}$$

where L represents the half thickness of the shear layer. There is a low-density plasma flowing in the $+x$ direction in the lower-part of the simulation domain ($y < 0$) and a high-density plasma at rest in the upper-part of the simulation domain ($y > 0$). In the two-dimensional coordinate system without an initial in-plane ambient magnetic field, the ordinary light-mode waves, which are responsive to the plasma motion in the out-of-plane direction, do not develop on the MHD scale. Hence, we neglect the third velocity dimension v_z in the present transverse KHI,[10,36] which substantially reduces the computational cost of Vlasov simulations.

Two simulation runs with $\boldsymbol{\Omega} \cdot \boldsymbol{B} > 0$ and $\boldsymbol{\Omega} \cdot \boldsymbol{B} < 0$ were performed to see the effect of the ion gyromotion. Since the vorticity of the initial primary velocity shear is set to be positive in the present simulation runs, the polarity of $\boldsymbol{\Omega} \cdot \boldsymbol{B}$ is controlled by the direction of the out-of-plane magnetic field B_z.

The velocity difference and the density ratio is given as $\Delta U = V_A = 4v_{ti}$ and $N_{low}/N_{high} = 0.1$, respectively, where $V_A = B_0/\sqrt{\mu_0 m_i N_{high}}$ is the Alfvén velocity in the high-density region. The initial half thickness of the shear layer is set as $L = d_i = 4r_i$, where $d_i \equiv c/\omega_{pi}$ and $r_i \equiv v_{ti}/\omega_{ci}$ represent the ion inertial length and the ion thermal gyroradius, respectively. Then, the wavelength of the most linearly unstable KH mode with these parameters corresponds to $\lambda_{KH} \approx 12L$, which is much longer than both ion inertial length and ion gyroradius ($\lambda_{KH} \sim 9.3d_i \sim 112.4r_i$ at $y = 0$). Therefore, the primary KHI is in the MHD regime. The KHI is initiated by a seed perturbation in the bulk velocity U_y component at the wavelength of $\lambda_{KH} = 12L$ in the x direction, with a amplitude of $\delta U_y = 0.01\Delta U$, which is a tenth of that in the previous study.[36] The ion cyclotron frequency ratio is $|\omega_{ci}|/\omega_{pi} = 0.05$, and the speed of light is $c/v_{ti} = 80.0$, where ω_{pi} and v_{ti} are the ion plasma frequency and thermal velocity in the high-density region. The plasma beta (the ratio of the thermal energy density to the magnetic energy density) is $\beta_i = \beta_e = 0.125$. A small ion-to-electron mass ratio $m_i/m_e = 25$ is used for the computational cost. The grid spacing is set as $\Delta = 2.0v_{ti,e}/\omega_{pi,e} = 0.5r_e = 0.125l_e = 0.1r_i = 0.025l_i$.

The initial density, bulk velocity, and temperature of ions and electrons are determined based on a two-fluid equilibrium. It should be noted that since the initial velocity distributions of the ions and electrons are isotropic Maxwellian, the initial condition is not a Vlasov equilibrium.

It should be noted that the deviation of the initial condition from the Vlasov–Maxwell equilibrium due to the fluid equilibrium results in an oscillation at mode 0 in the x direction with an amplitude of $\sim 0.1\Delta U$.[33,35] The thickness of the initial velocity shear layer increases by 6% for the simulation run with $\boldsymbol{\Omega} \cdot \boldsymbol{B} > 0$ and by 20% for the simulation run with $\boldsymbol{\Omega} \cdot \boldsymbol{B} < 0$. We adopt the two-fluid equilibrium to satisfy the frozen-in condition $\boldsymbol{E} = -\boldsymbol{U}_s \times \boldsymbol{B}$, Gauss's law $\nabla \cdot \boldsymbol{E} = \rho/\epsilon_0$, and Ampère's law $\nabla \times \boldsymbol{B} = \mu_0 \boldsymbol{J}$ simultaneously. Since the spatial profiles of the charge and current densities based on the Vlasov equilibrium with the homogeneous ambient magnetic field[48,49] have deviations from the analytic form obtained from Eqs. (34) and (35), it is quite difficult to satisfy the three constraints, i.e., the frozen-in condition, Gauss's law, and Ampère's law.

IV. RESULTS

Figures 1 and 2 show the third moment of ions around the saturation stage of the transverse KHI for the simulation run with
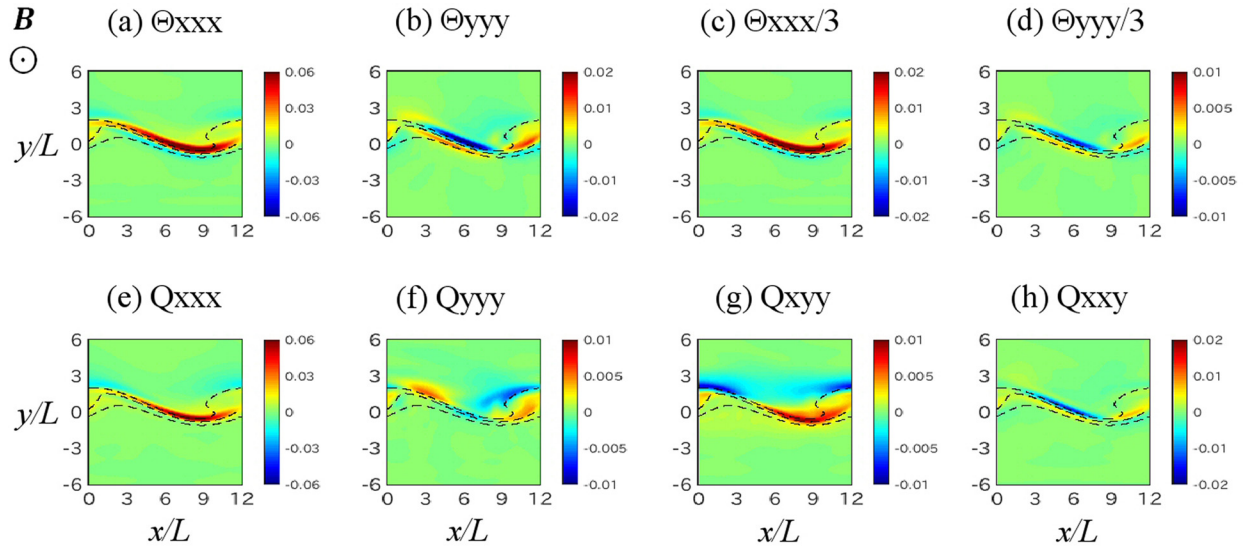
FIG. 1. Spatial profiles of Θ_{xxx}, Θ_{yyy}, $\Theta_{xxx}/3 (= \Theta_{xyy})$, $\Theta_{yyy}/3 (= \Theta_{xxy})$, Q_{xxx}, Q_{yyy}, Q_{xyy}, and Q_{xxy} for the run with $\boldsymbol{\Omega} \cdot \boldsymbol{B} > 0$ at $\omega_{ci}t = 80$.

$\boldsymbol{\Omega} \cdot \boldsymbol{B} > 0$ at $\omega_{ci}t = 80$ and $\boldsymbol{\Omega} \cdot \boldsymbol{B} < 0$ at $\omega_{ci}t = 110$, respectively. The panels (a)–(d) show Θ_{xxx}, Θ_{yyy}, $\Theta_{xxx}/3 (= \Theta_{xyy})$, and $\Theta_{yyy}/3$ $(= \Theta_{xxy})$, respectively, which are calculated by using the moment data in the Vlasov simulation based on Eqs. (30) and (31). The panels (e)–(h) show the heat flux Q_{xxx}, Q_{yyy}, Q_{xyy}, and Q_{xxy}, respectively, which are calculated directly from the ion velocity distribution in the Vlasov simulation. The magnitude is normalized by $m_e N_e V_{te}^3$. The dashed lines show the contour lines of the ion density as a reference to the primary KH vortex.

The spatial profile of Θ_{xxx} in Figs. 1 and 2 is similar to that of Q_{xxx} in both runs. By contrast, the spatial profile of Θ_{yyy} is quite different from that of Q_{yyy} in the run with $\boldsymbol{\Omega} \cdot \boldsymbol{B} > 0$. Although the spatial

profile of Θ_{yyy} is similar to that of Q_{yyy} in the run with $\boldsymbol{\Omega} \cdot \boldsymbol{B} < 0$, on the other hand, the magnitude is about half. The spatial profile of $\Theta_{xyy}(= \Theta_{xxx}/3)$ is quite different from that of Q_{xyy} in the run with $\boldsymbol{\Omega} \cdot \boldsymbol{B} > 0$. On the other hand, the spatial profile of Θ_{xyy} is similar to that of Q_{xyy} in the run with $\boldsymbol{\Omega} \cdot \boldsymbol{B} < 0$, except their magnitude. The spatial profile of $\Theta_{xxy}(= \Theta_{yyy}/3)$ is similar to that of Q_{xxy} in both runs. Figures 1 and 2 clearly show $Q_{xyy} \neq Q_{xxx}/3$ and $Q_{xxy} \neq Q_{yyy}/3$ as well. These results suggest that Eqs. (15)–(18) based on the procedure of Thompson[4] are not good approximations of the third moment (i.e., heat flux tensor). It is noted that the difference between $\boldsymbol{\Theta}$ and $\boldsymbol{Q}$ becomes larger with Eqs. (20) and (21) than with $mNdU_x/dt \approx -\partial P/\partial x$ and $mNdU_y/dt \approx -\partial P/\partial y$.
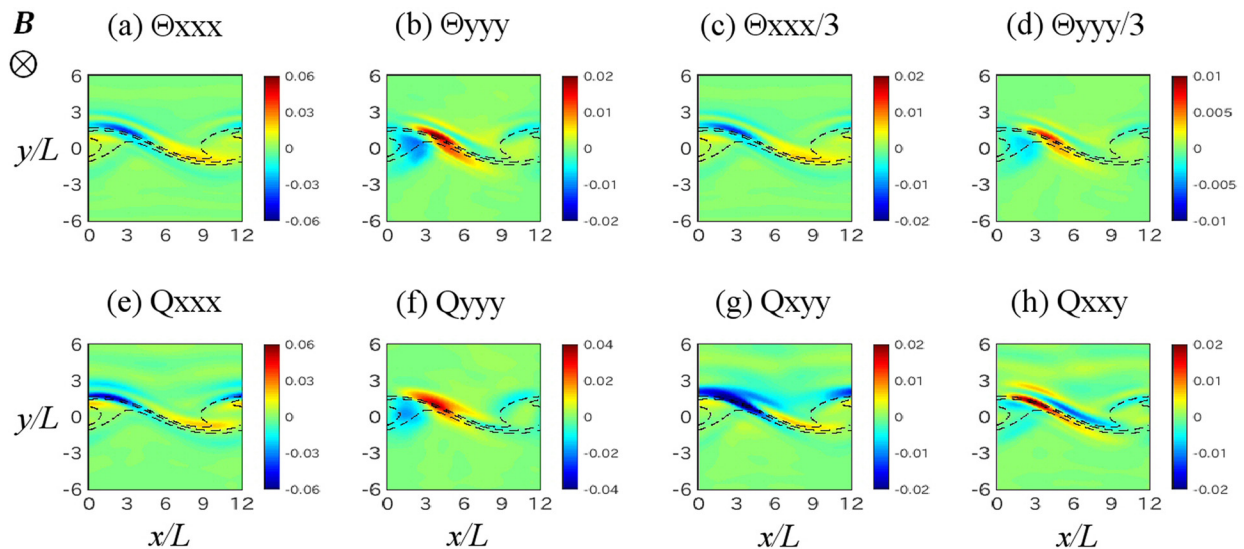
FIG. 2. Same format as Fig. 1 for the run with $\boldsymbol{\Omega} \cdot \boldsymbol{B} < 0$ at $\omega_{ci}t = 110$.
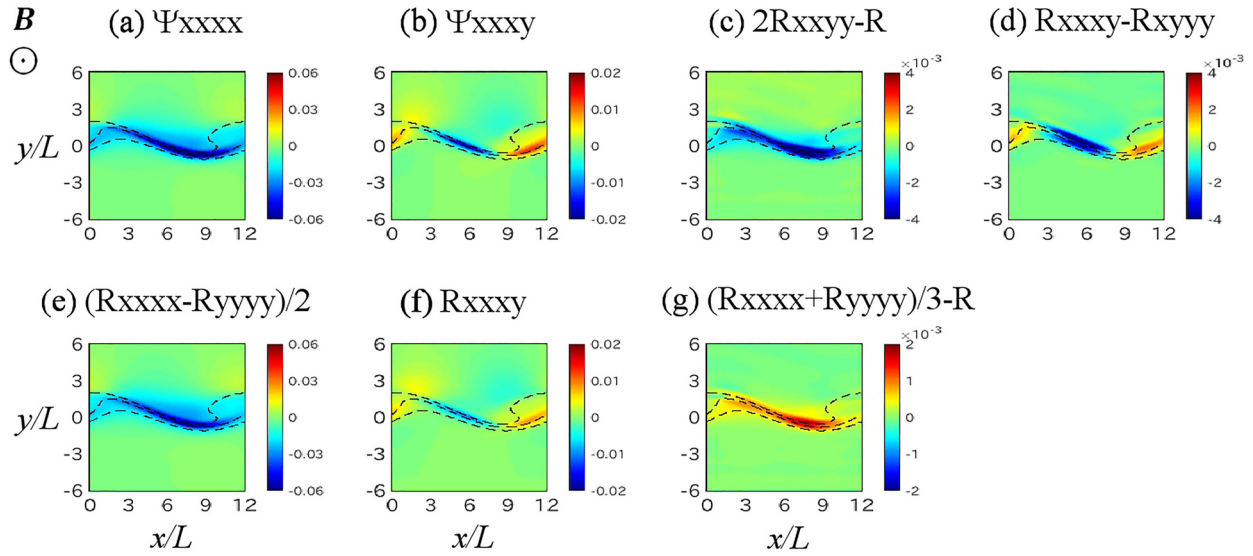
FIG. 3. Spatial profiles of Ψ_{xxxx}, Ψ_{xxxy}, $2R_{xxyy} - R$, $R_{xxxy} - R_{xyyy}$, $(R_{xxxx} - R_{yyyy})/2$, R_{xxxy}, and $(R_{xxxx} + R_{yyyy})/3 - R$ for the run with $\mathbf{\Omega} \cdot \mathbf{B} > 0$ at $\omega_{ci}t = 80$.

Figures 3 and 4 show the fourth moment of ions around the saturation stage for the simulation run with $\mathbf{\Omega} \cdot \mathbf{B} > 0$ at $\omega_{ci}t = 80$ and $\mathbf{\Omega} \cdot \mathbf{B} < 0$ at $\omega_{ci}t = 110$, respectively. The panels (a) and (b) show $\Psi_{xxxx}(= -\Psi_{yyyy})$ and $\Psi_{xxxy}(= \Psi_{xyyy})$, respectively, which are calculated by using the moment data in the Vlasov simulation based on Eqs. (32) and (33). The panels (e) and (f) show the fourth moment $(R_{xxxx} - R_{yyyy})/2$ and R_{xxxy}, respectively, which are calculated directly from the ion velocity distribution in the Vlasov simulation. The panels (c), (d), and (g) show the differences $2R_{xxyy} - R$, $R_{xxxy} - R_{xyyy}$, and

$(R_{xxxx} + R_{yyyy})/3 - R$, respectively. The magnitude is normalized by $m_e N_e V_{te}^4$. The dashed lines show the contour lines of the ion density.

In contrast to the third moment in Figs. 1 and 2, the spatial profile of Ψ_{xxxx} and Ψ_{xxxy} in Figs. 3 and 4 are similar to that of $(R_{xxxx} - R_{yyyy})/2$ and R_{xxxy}, respectively, in both runs. There is a difference of about 30% in the magnitude between them. Although Eq. (26) gives $2R_{xxyy} = R$, Figs. 3 and 4 show that there is a difference, of about 7% in the magnitude, between $2R_{xxyy}$ and R. Also, although Eq. (24) plus Eq. (28) gives $(R_{xxxx} + R_{yyyy})/3 = R$, there is a difference,
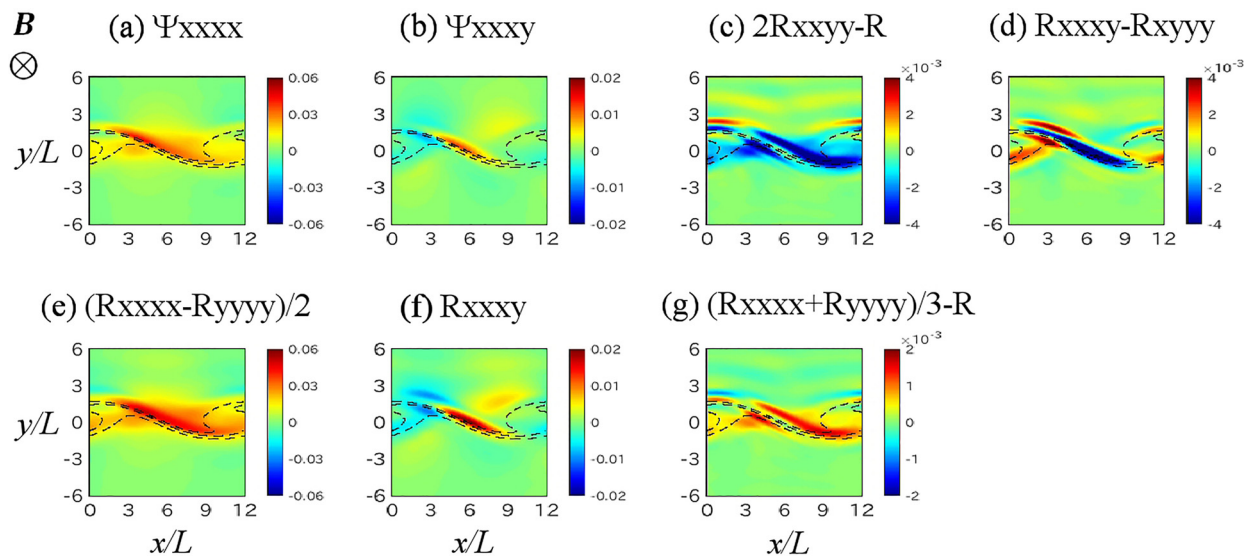
FIG. 4. Same format as Fig. 3 for the run with $\mathbf{\Omega} \cdot \mathbf{B} < 0$ at $\omega_{ci}t = 110$.

of about 4% in the magnitude, between $(R_{xxxx} + R_{yyyy})/3$ and R. Note that the difference between R_{xxxx} (or R_{yyyy}) and $3R/2\pm\Psi_{xxxx}$ is also small (about 4% in the magnitude). In addition, although Eqs. (25) and (27) give $R_{xxxy} = R_{xyyy}$, there is a difference, of about 30% in the magnitude, between R_{xxxy} and R_{xyyy}. These results suggest that Eqs. (24)–(28) based on the procedure of Thompson[4] are good (but not excellent) approximations of the fourth moment.

The previous study[1] showed that the approximated form of the second moment derived by Thompson[4] was in agreement (but not excellent) with the pressure/stress tensor calculated directly from the ion distribution function of the Vlasov simulation. The terms (a) in Eq. (12) vanish in even-number-order moments, while the terms (b) vanish in odd-number-order moments due to the integration over the gyrophase θ. The present and previous[1] results indicate that the terms (b) in Eq. (12) well approximate the first-order perturbation of a velocity distribution function around a characteristic spatial scale on the gyroradius, while the terms (a) do not.

V. CONCLUSION

In the present study, the gyro-averaging approximation of the third and fourth moments of a velocity distribution function is derived by using a procedure of the past study.[4] Then, the derived approximated forms are directly compared with the two-dimensional full Vlasov simulation results of the transverse KHI.

It is shown that the approximated form of the third moment is quite different from the third moment (i.e., heat flux tensor) calculated directly from the distribution function data of the Vlasov simulation. By contrast, the approximated form of the fourth moment is in agreement with the fourth moment calculated directly from the distribution function data of the Vlasov simulation. The latter result is similar to the previous study,[1] which showed that the gyro-averaging form of the second moment derived by Thompson[4] is a good approximation of the second moment (i.e., pressure/stress tensor) calculated directly from the distribution function data of the Vlasov simulation.

The present result suggests that the first-order approximation of a perturbed velocity distribution function around a characteristic spatial scale on gyroradius in Eq. (12) needs an improvement. In particular, the terms (a) in Eq. (12), which are related to odd-number-order moments, need re-examination. It is also unclear whether the present result is universal or specific for the KHI only, because $\partial P/\partial y$, $\partial R/\partial y$, and $\partial U_x/\partial y$ are dominant in the present simulation setup. The evaluation of the third and fourth moments with different fluid instabilities at boundary layers is left as future studies.

ACKNOWLEDGMENTS

REFERENCES

[1] T. Umeda, N. Yamauchi, Y. Wada, and S. Ueno, Phys. Plasmas **23**, 054506 (2016).

[2] T. Umeda and Y. Wada, Phys. Plasmas **23**, 112117 (2016).

[3] T. Umeda and Y. Wada, Phys. Plasmas **24**, 072307 (2017).

[4] W. B. Thompson, Rep. Prog. Phys. **24**, 363–424 (1961).

[5] K. V. Roberts and J. B. Taylor, Phys. Rev. Lett. **8**, 197–198 (1962).

[6] A. Miura, Phys. Rev. Lett. **49**, 779–782 (1982).

[7] A. Miura, J. Geophys. Res. **97**(10), 10655–10675, https://doi.org/10.1029/92JA00791 (1992).

[8] A. Otto and D. H. Fairfield, J. Geophys. Res. **105**, 21175–21190, https://doi.org/10.1029/1999JA000312 (2000).

[9] H. Baty, R. Keppens, and P. Comte, Phys. Plasmas **10**, 4661–4676 (2003).

[10] M. Faganello and F. Califano, J. Plasma. Phys. **83**, 535830601 (2017).

[11] S. Fadanelli, M. Faganello, F. Califano, S. S. Cerri, F. Pegoraro, and B. Lavraud, J. Geophys. Res. **123**, 9340–9356, https://doi.org/10.1029/2018JA025626 (2018).

[12] D. H. Fairfield, A. Otto, T. Mukai, S. Kokubun, R. P. Lepping, J. T. Steinberg, A. J. Lazarus, and T. Yamamoto, J. Geophys. Res. **105**, 21159, https://doi.org/10.1029/1999JA000316 (2000).

[13] H. Hasegawa, M. Fujimoto, T.-D. Phan, H. Reme, A. Balogh, M. W. Dunlop, C. Hashimoto, and R. TanDokoro, Nature **430**, 755 (2004).

[14] C. Foullon, C. J. Farrugia, A. N. Fazakerley, C. J. Owen, F. T. Gratton, and R. B. Torbert, J. Geophys. Res. **113**, A11203, https://doi.org/10.1029/2008JA013175 (2008).

[15] H. Hasegawa, A. Retinò, A. Vaivads, Y. Khotyaintsev, M. André, T. K. M. Nakamura, W.-L. Teh, B. U. Ö. Sonnerup, S. J. Schwartz, Y. Seki, M. Fujimoto, Y. Saito, H. Rème, and P. Canu, J. Geophys. Res. **114**, A12207, https://doi.org/10.1029/2009JA014042 (2009).

[16] M. Faganello, F. Califano, F. Pegoraro, and A. Retinó, Europhys. Lett. **107**, 19001 (2014).

[17] J. R. Johnson, S. Wing, and P. A. Delamere, Space Sci. Rev. **184**, 1–31 (2014).

[18] Y. Matsumoto and M. Hoshino, Geophys. Res. Lett. **31**, L02807, https://doi.org/10.1029/2003GL018195 (2004).

[19] M. Faganello, F. Califano, and F. Pegoraro, Phys. Rev. Lett. **100**, 015001 (2008).

[20] A. Tenerani, M. Faganello, F. Califano, and F. Pegoraro, Plasma Phys. Controlled Fusion **53**, 015003 (2011).

[21] Y. Matsumoto and K. Seki, J. Geophys. Res. **112**, A06223, https://doi.org/10.1029/2006JA012114 (2007).

[22] T. K. M. Nakamura, D. Hayashi, M. Fujimoto, and I. Shinohara, Phys. Rev. Lett. **92**, 145001 (2004).

[23] J. Dargent, F. Lavorenti, F. Califano, P. Henri, F. Pucci, and S. S. Cerri, J. Plasma Phys. **85**, 805850601 (2019).

[24] K. Nykyri and A. Otto, Geophys. Res. Lett. **28**, 3565–3568, https://doi.org/10.1029/2001GL013239 (2001).

[25] T. K. M. Nakamura and M. Fujimoto, Geophys. Res. Lett. **32**, L21102, https://doi.org/10.1029/2005GL023362 (2005).

[26] T. K. M. Nakamura and M. Fujimoto, Phys. Rev. Lett. **101**, 165002 (2008).

[27] M. Faganello, F. Califano, and F. Pegoraro, Phys. Rev. Lett. **101**, 105001 (2008).

[28] M. Faganello, F. Califano, and F. Pegoraro, Phys. Rev. Lett. **101**, 175003 (2008).

[29] T. K. M. Nakamura, H. Hasegawa, I. Shinohara, and M. Fujimoto, J. Geophys. Res. **116**, A03227, https://doi.org/10.1029/2010JA016046 (2011).

[30] T. K. M. Nakamura, W. Daughton, H. Karimabadi, and S. Eriksson, J. Geophys. Res. **118**, 5742, https://doi.org/10.1002/jgra.50547 (2013).

[31] M. Wilber and R. M. Winglee, J. Geophys. Res. **100**, 1883–1898, https://doi.org/10.1029/94JA02488 (1995).

[32] J. D. Huba, Geophys. Res. Lett. **23**, 2907–2910, https://doi.org/10.1029/96GL02767 (1996).

[33] T. K. M. Nakamura, H. Hasegawa, and I. Shinohara, Phys. Plasmas **17**, 042119 (2010).

[34] P. Henri, S. S. Cerri, F. Califano, F. Pegoraro, C. Rossi, M. Faganello, O. Sebek, P. M. Travnicek, P. Hellinger, J. T. Frederiksen, A. Nordlund, S. Markidis, R. Keppens, and G. Lapenta, Phys. Plasmas **20**, 102118 (2013).

[35] S. S. Cerri, P. Henri, F. Califano, D. Del Sarto, M. Faganello, and F. Pegoraro, Phys. Plasmas **20**, 112112 (2013).

[36] T. Umeda, S. Ueno, and T. K. M. Nakamura, Plasma Phys. Controlled Fusion **56**, 075006 (2014).

[37] S. S. Cerri, F. Pegoraro, F. Califano, D. Del Sarto, and F. Jenko, Phys. Plasmas **21**, 112109 (2014).

[38] S. De Camillis, S. S. Cerri, F. Califano, and F. Pegoraro, Plasma Phys. Controlled Fusion **58**, 045007 (2016).

[39] S. S. Cerri, J. Plasma Phys. **84**, 555840501 (2018).

[40] A. Macmahon, Phys. Fluids **8**, 1840–1845 (1965).

[41] Y. C. Whang, J. Geophys. Res. **76**, 7503–7507, https://doi.org/10.1029/JA076i031p07503 (1971).

[42] T. Umeda, J. Miwa, Y. Matsumoto, T. K. M. Nakamura, K. Togano, K. Fukazawa, and I. Shinohara, Phys. Plasmas **17**, 052311 (2010).

[43] T. Umeda, Earth Planets Space **60**, 773–779 (2008).

[44] T. Umeda, Y. Nariyuki, and D. Kariya, Comput. Phys. Commun. **183**, 1094–1100 (2012).

[45] H. Schmitz and R. Grauer, Comput. Phys. Commun. **175**, 86–92 (2006).

[46] T. Umeda, K. Togano, and T. Ogino, Comput. Phys. Commun. **180**, 365–374 (2009).

[47] T. Umeda, K. Fukazawa, Y. Nariyuki, and T. Ogino, IEEE Trans. Plasma Sci. **40**, 1421–1428 (2012).

[48] D. Cai, L. R. O. Storey, and T. Neubert, Phys. Fluids B **2**, 75–85 (1990).

[49] F. Malara, O. Pezzi, and F. Valentini, Phys. Rev. E **97**, 053212 (2018).